Astronomy & Astrophysics manuscript no. 12484
January 6, 2010

H_2CO and CH_3OH maps of the Orion Bar photodissociation region⋆

S. Leurini[1,2], B. Parise[2], P. Schilke[2,3], J. Pety[4], R. Rolffs[2]

[1] ESO, Karl-Scharzschild-Strasse 2, D-85748, Garching-bei-München, Germany
e-mail: sleurini@mpifr.de
[2] Max-Planck-Institut für Radioastronomie, Auf dem Hügel 69, 53121 Bonn, Germany
[3] Physikalisches Institut, Universität zu Köln, Zülpicher Str. 77, 50937 Köln, Germany
[4] Institut de Radioastronomie Millimétrique, 300 Rue de la Piscine, 38406 Saint Martin d'Hères, France

January 6, 2010

ABSTRACT

Context. A previous analysis of methanol and formaldehyde towards the Orion Bar concluded that the two molecular species may trace different physical components, methanol the clumpy material, and formaldehyde the interclump medium.
Aims. To verify this hypothesis, we performed multi-line mapping observations of the two molecules to study their spatial distributions.
Methods. The observations were performed with the IRAM-30m telescope at 218 and 241 GHz, with an angular resolution of ∼ 11″. Additional data for H_2CO from the Plateau de Bure array are also discussed. The data were analysed using an LVG approach.
Results. Both molecules are detected in our single-dish data. Our data show that CH_3OH peaks towards the clumps of the Bar, but its intensity decreases below the detection threshold in the interclump material. When averaging over a large region of the interclump medium, the strongest CH_3OH line is detected with a peak intensity of ∼ 0.06 K. Formaldehyde also peaks on the clumps, but it is also detected in the interclump gas.
Conclusions. We verified that the weak intensity of CH_3OH in the interclump medium is not caused by the different excitation conditions of the interclump material, but reflects a decrease in the column density of methanol. The abundance of CH_3OH relative to H_2CO decreases by at least one order of magnitude from the dense clumps to the interclump medium.

Key words. ISM: individual objects (Orion Bar) - ISM: abundances - ISM: molecules - ISM: structure

1. Introduction

Given its proximity and nearly edge-on orientation, the so-called Orion Bar is one of the clearest examples of a photon-dominated region (PDR). For this reason, the Orion Bar has been extensively observed in past decades to test theoretical models of PDR structure, chemistry, and energetics. Its nearly edge-on orientation make direct observations of the gas stratification possible, from ionised gas to neutral atomic gas to molecular gas as a function of the increasing distance from the ionisation source (e.g., Tielens et al. 1993; van der Werf et al. 1996; van der Wiel et al. 2009). These studies show that the molecular gas consists of clumpy molecular cores embedded in an interclump gas. While the clumps have densities of several 10^6 cm^{-3} (Young Owl et al. 2000; Lis & Schilke 2003), the interclump material has lower densities (10^4–10^5 cm^{-3}, Hogerheijde et al. 1995; Young Owl et al. 2000). Such observational results are successfully reproduced by theoretical works (e.g., Gorti & Hollenbach 2002).

Observations of methanol (CH_3OH) and formaldehyde (H_2CO) in the Orion Bar have been reported in the past (Hogerheijde et al. 1995; Jansen et al. 1995; Leurini et al. 2006). Leurini et al. (2006) studied the excitation of both molecular species in the line of sight of one molecular clump through a multi-line analysis at 290 GHz. Their findings (high density and relatively low temperature for CH_3OH, high temperature, and relatively low density for H_2CO) suggest that methanol and formaldehyde do not trace the same material, but the first is found in the dense gas associated with the clumps, the second in the warmer and less dense gas of the interclump material. Since both molecular species can efficiently form on grain surfaces (Hidaka et al. 2004), the authors suggested that photodissociation of methanol to form formaldehyde (Le Teuff et al. 2000) takes place in the interclump medium, while the high density shields CH_3OH in the clumps and prevents its photodissociation. Whereas grain surface reactions are the only viable route to methanol, formaldehyde can also form in the gas phase via the reaction CH_3+O (e.g., Le Teuff et al. 2000), which could contribute to the interclump abundance of H_2CO.

However, the study of Leurini et al. (2006) on CH_3OH and H_2CO is based on low angular resolution (∼ 20″), single-pointing data. To confirm that the two species indeed trace different media, we mapped a large area of the Orion Bar in formaldehyde and methanol at 218 and 241 GHz, respectively, with an angular resolution of ∼ 11″. We also analysed existing interferometric data for the 218 GHz formaldehyde lines, to compare the observed fluxes from single-dish and interferometer and derive constraints on the size of the emitting region. This work represents a first observational attempt to study the distribution of CH_3OH and H_2CO in the Orion Bar and to verify their different origin.

Send offprint requests to: S. Leurini

⋆ Based on observations carried out with the IRAM-30m telescope and the Plateau de Bure interferometer. IRAM is supported by INSU/CNRS (France), MPG (Germany) and IGN (Spain).

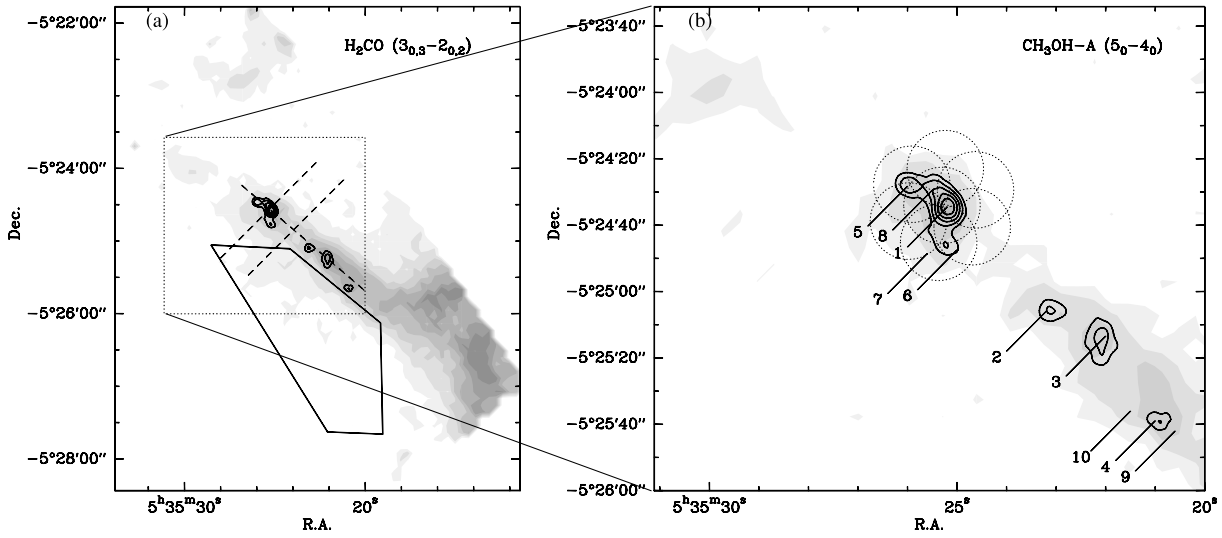

(a)

Fig. 1. In grey scale, the integrated intensity of the H_2CO ($3_{0,3} - 2_{0,2}$) line (left) and of the CH_3OH-*A* ($5_0 - 4_0$) transition (right) observed with the IRAM-30m telescope. Black contours (4, 8, and 12 times 0.032 Jy beam^{-1} km s^{-1}) show the distribution of the $H^{13}CN$ (1-0) emission observed with the Plateau de Bure interferometer (Lis & Schilke 2003). For H_2CO the contours start from 1.8 K km s^{-1} in steps of 1.8 (equal to 3σ), for CH_3OH from 0.3 K km s^{-1} in steps of 0.3 (equal to 3σ). In the left panel, the dashed lines indicate the strips used for Fig. 6; the solid lines outline the regions used to derive the average H_2CO and CH_3OH emission in the interclump material (Figs. 3(b) and 4(c)); the dotted lines mark the region shown in the right panel. In the right panel, the numbers label the positions of the clumps detected in $H^{13}CN$; the dotted circles outline the mosaic of seven fields observed with the PdBI (see § 2.2).

2. Observations

2.1. IRAM-30m telescope

The observations were performed in February and March 2007 using the HERA multi-beam receiver (Schuster et al. 2004) at the IRAM-30m telescope. The HERA1 and HERA2 pixels were tuned to 241.850 GHz in lower side band (LSB), to detect the CH_3OH ($5_k - 4_k$) band. On February 23 and 24, the HERA2 receivers were tuned to 218.349 GHz (LSB) to detect the H_2CO ($3_{K_a,K_c} - 2_{K_a,K_c-1}$) band. The backend used was VESPA with a bandwidth of 160 MHz and a resolution of 0.3125 MHz for the CH_3OH setup (corresponding to a velocity resolution of $\sim$ 0.4 km s^{-1}), 160 MHz and 1.25 MHz for the H_2CO setup (corresponding to $\sim$ 1.7 km s^{-1}). In this way, the CH_3OH ($5_k - 4_k$) band is fully covered with the only exception being the $k = -1, 0$-*E* lines. The H_2CO setup covers the $3_{0,3} - 2_{0,2}$ and $3_{2,2} - 2_{2,1}$ lines, while the $3_{2,1} - 2_{2,0}$ transition lies outside the observed frequency range.

We used the on-the-fly mode with a rotation of the multi-beam system of 9.7°, to ensure a Nyquist sampling between the rows. The reference position used as the centre of the map was $\alpha_{2000} = 05^h35^m25^s.3, \delta_{2000} = -05°24'34''.0$, corresponding to the "Orion Bar (HCN)" position of Schilke et al. (2001), the most massive clump seen in $H^{13}CN$ (Lis & Schilke 2003), as well as the target of the spectral survey of Leurini et al. (2006). The OFF position was chosen to be $(500'', 0'')$ from the centre of the map.

The pointing was checked on several continuum sources and found to be accurate within 2″. The observations were done under varying weather conditions, and the T_{sys} span the range 540–1200 K for HERA1 and 700–1600 K for HERA2. The half-power beam width of the IRAM-30m telescope at 218 GHz is $\sim$ 11″ and $\sim$ 10″ at 242 GHz. We used a beam efficiency of 0.55 at 218 GHz, and of 0.50 at 242 GHz to convert antenna temperatures $T_a^\star$ into main-beam temperatures T_{mb}[1].

The region covered by our observations is shown in Fig. 1.

2.2. Plateau de Bure interferometer

We observed the H_2CO $3_{0,3} - 2_{0,2}$ line at 218.2 GHz with the Plateau de Bure interferometer in March, April, and December 2004. We observed a 7-field mosaic centred on $\alpha_{2000} = 05^h35^m25.280^s$, $\delta_{2000} = -05°24'39''.300$. The field positions followed a compact hexagonal pattern to ensure Nyquist sampling in all directions. The imaged field-of-view is almost a circle with a radius of 22.5″. On March 28 and 29, the six antennas were used in the 6 Cp configuration with 3 and 1.5 mm precipitable water vapour, which translated into system temperatures of 450 K and 250 K. On April 22, the six antennas were used in the more compact 6Dp configuration with 6 to 10 mm PWV, leading to a system temperature of about 1000 K. On December 12, the six antennas were used in the 6Cp configuration, with 3.5 mm PWV, leading to a system temperature of about 700 K. Taking the time for calibration and data filtering into account, this translates into an *on–source* integration time of useful data of 5.3 hours for a full 6-antenna array. The typical 1 mm resolution is 2.4″. We used the 30m data described above to produce the missing short spacings.

The data processing was done with the GILDAS[2] software suite (Pety 2005). Standard calibration methods implemented in the GILDAS/CLIC program were applied using close bright quasars (0528+134 and 0607−157) as phase and amplitude calibrators. The absolute flux was calibrated using simultaneous

[1] http://www.iram.es/IRAMES/telescope.html

[2] See `http://www.iram.fr/IRAMFR/GILDAS` for more information about the GILDAS softwares.

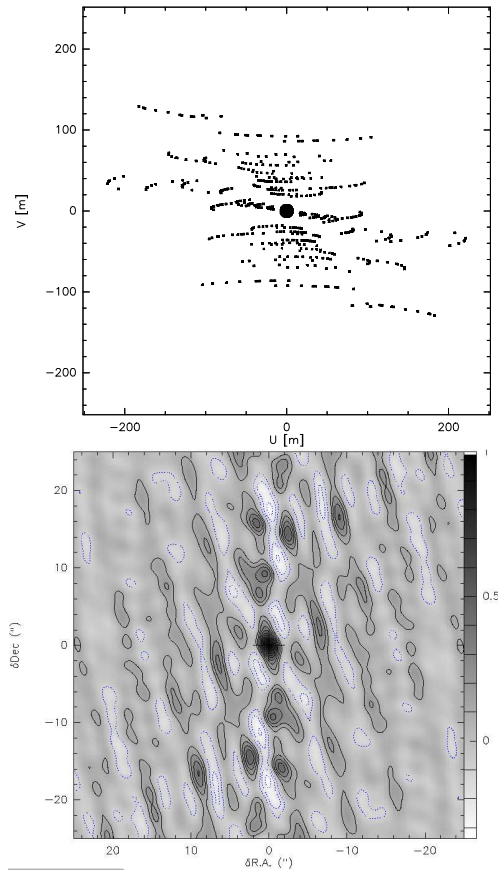

Fig. 2. *Top: uv* coverage for one field of the hybrid 30m+PdBI mosaic. *Bottom:* Associated dirty beam. Please note that the dirty beam has many secondary side-lobes as high as 40% of the main lobe.

measurements of the PdBI primary flux calibrator MWC349. *uv* tables were then produced at a relatively coarse velocity resolution of 1.7 km/s.

All other processing was performed with the GILDAS/MAPPING software. The single-dish map from the IRAM-30m was used to create the short-spacing pseudo-visibilities unsampled by the Plateau de Bure interferometer (Rodríguez-Fernández et al. 2008). These were then merged with the interferometric observations. Each mosaic field was imaged independently, and a dirty mosaic was built through a linear combination of these dirty images (Gueth et al. 1995). The dirty mosaic was then deconvolved using the standard Högbom CLEAN algorithm. While all these procedures are standard and usually easy to use in the GILDAS/MAPPING software, we had to take special precautions with this data set because the short usable integration time at PdBI implied 1) a low signal-to-noise ratio of the interferometric data and 2) dirty beams for each field with large secondary side-lobes (see Fig. 2). As the 30m data show that the extended signal fills most of the field-of-view observed with the interferometer, we subtracted the spectrum averaged over the observed field-of-view from the 30m data before any processing and we added this averaged spectrum again after the deconvolution of the 30m+PdBI hybrid data set to recover the correct flux scale. This simplifies the deconvolution considerably by the usual CLEAN algorithms (*i.e.* much fewer CLEAN components are needed) because it avoids the deconvolution of extended uniform intensities. Second, we tapered the visibility weights

Table 1. Detected methanol and formaldehyde transitions in the IRAM-30m telescope data

line	ν [MHz]	E_{up} [K]	clump 1	interclump
H_2CO $3_{0,3}-2_{0,2}$	218222	21.0	Y[a]	Y
H_2CO $3_{2,2}-2_{1,1}$	218475	68.0	Y[a]	Y
CH_3OH-A 5_0-4_0	241791	34.8	Y[a]	Y
CH_3OH-A $5_{\pm3}-4_{\pm3}$	241832	84.6	Y[b]	N
CH_3OH-A 5_2-4_2	241842[c]	72.5	Y[b]	N
CH_3OH-E 5_3-4_3	241843	82.5	Y[b]	N
CH_3OH-E 5_1-4_1	241879	55.9	Y[a]	N
CH_3OH-E $5_{\pm2}-4_{\pm2}$	241904	~ 60[d]	Y[b]	N

[a] detected at the original resolution of the IRAM-30m telescope data
[b] detected at a resolution of $\sim 20''$
[c] blended with the 5_3-4_3-E
[d] E_{up} =60.7 K for the $5_{-2}-4_{-2}$ line, 57.1 K for the $5_{+2}-4_{+2}$ transition.

with an axis-symmetrical Gaussian of 80m *FWHM* to get a more symmetrical beam (going from $4.1''\times1.2''$ for natural weighting to $3.3''\times1.8''$ after tapering) and to improve the signal-to-noise ratio for the extended structures. The final noise rms measured at the centred of the mosaic is about 0.3 K in channels of 1.7 km/s width. This leads to a maximum signal-to-noise ratio of 18 for the hybrid data cube. However, the produced data cube has its brightness dynamical range limited by the poor dirty beam. The cleaned data cube was finally scaled from Jy/beam to T_{mb} temperature scale using the synthesised beam size.

3. Observational results

3.1. single-dish data

Figures 3(a) and 4(a) show the spectra at 218.4 and 241.8 GHz towards the central position of the map. Both formaldehyde transitions are detected. Only the 5_0-4_0-A and 5_1-4_1-E methanol transitions are detected at the original resolution of $\sim 10''$. However, when increasing the signal-to-noise ratio by smoothing to a lower resolution of $\sim 20''$, CH_3OH transitions with upper level energies lower than 85 K are also detected (Fig. 4(b)). The detected lines of both molecular species are reported in Table 1.

The region mapped with the IRAM-30m telescope is presented in Fig. 1, where in the left panel we show the integrated intensity of the strongest detected H_2CO line, while the right panel shows the emission from the strongest CH_3OH transition along the Orion Bar alone. For comparison, the integrated intensity of the $H^{13}CN$ (1-0) from Lis & Schilke (2003) is overlaid on our data. Both molecules clearly trace the molecular medium associated with the Orion Bar, and peak to the southwest of it. This peak probably belongs to the low-intensity bridge that connects Orion South to the Orion Bar. This structure was detected in previous observations at velocities between 7 and 9 km s^{-1} (e.g., Tauber et al. 1995). The southwest peak of CH_3OH and H_2CO detected in our data has a peak velocity of 8 km s^{-1}. In addition, formaldehyde is detected towards the north of the map, at a position that spatially coincides with continuum emission at 350 μm (Lis et al. 1998) and with a velocity between 9 and 11 km s^{-1}.

Along the Bar, both molecules trace the elongated region where molecular clumps are located, with an absolute emis-

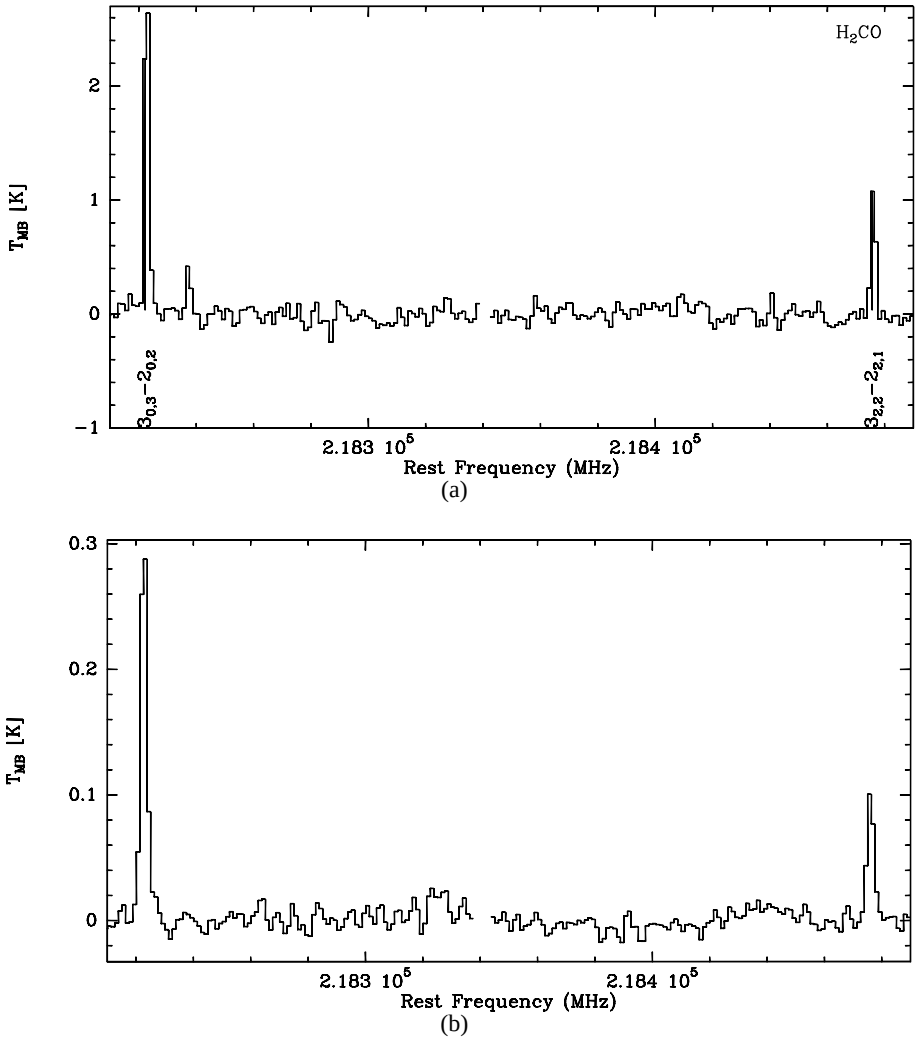

Fig. 3. Spectrum of the H_2CO ($3_{K_a,K_c} - 2_{K_a,K_c-1}$) band towards clump 1 (top) and averaged over the interclump medium (bottom) from the IRAM-30m telescope.

sion peak on clump 3 of Lis & Schilke (2003). Moreover, both species are detected on a secondary peak, northeast of clump 1 ($\alpha_{2000} = 05^h35^m29.6^s, \delta_{2000} = -05°23'59''.9$), not covered by the observations of Lis & Schilke (2003), but close to a peak of CO(6-5) (Fig. 5), which could represent an additional clump of dense gas along the Orion Bar. To better visualise the overall morphology of the Orion Bar, in Fig. 5 we show the 20 cm continuum emission from Yusef-Zadeh (1990), which traces the ionisation front; the CO(6-5) integrated emission (Lis et al. 1998), which shows the temperature distribution of the molecular gas; and the $H^{13}CN$ (1-0) emission, which traces the dense clumps.

In Fig. 3 and 4 we compare the H_2CO and CH_3OH spectrum towards clump 1 to the corresponding spectra averaged over the region of the interclump gas outlined in Fig. 1 (left). The integrated intensity of the CH_3OH ($5_0 - 4_0$)-*A* transition in the interclump medium is a factor $\sim$ 9 lower than in the clump, the one of H_2CO $3_{2,2} - 2_{2,1}$ line a factor of 7 (see Table 2). For a better visualisation of the formaldehyde and methanol morphologies, we show in Fig. 6 the variation in the integrated intensities of the CH_3OH-*A* ($5_0 - 4_0$) and H_2CO ($3_{2,2} - 2_{2,1}$) lines for three strips in the map; the exact location of the strips is shown in Fig. 1. The strip across clump 1 (Fig. 6(a)) suggests a larger extension of the H_2CO emission with respect to CH_3OH, while the variation in the integrated intensity of the two species along the Bar is very similar (Fig. 6(c)). Although we present data for the weakest of the two H_2CO lines, the signal-to-noise ratio in the methanol data is still lower than for H_2CO and could bias our results. From these strips and from the comparison between the H_2CO emission and the CO(6-5) map, it also emerges that formaldehyde extends to a greater distance from the clumps in the molecular cloud than towards the ionisation front. We also smoothed the data to lower resolutions, to verify whether the CH_3OH and H_2CO emission are similarly affected by beam dilution. At a resolution of 50″, the H_2CO emission is still $\sim$ 37% of the intensity of the original data, while at the same resolution the CH_3OH peak intensity drops down to $\sim$ 18% of the original value. These tests suggest that formaldehyde emission is associated with the clumps but also with the interclump medium, while methanol emission is only found in the dense molecular clumps. In Sect. 4, we investigate whether the different morphologies of the two molecular species stem from an excitational or observational bias, or whether they imply different abundances of H_2CO and CH_3OH in the two media.

Finally, the spectral resolution used for the methanol observations allows us to study the velocity field along the Bar. The channel maps of the ($5_0 - 4_0$)-*A* line (Fig. 7, smoothed

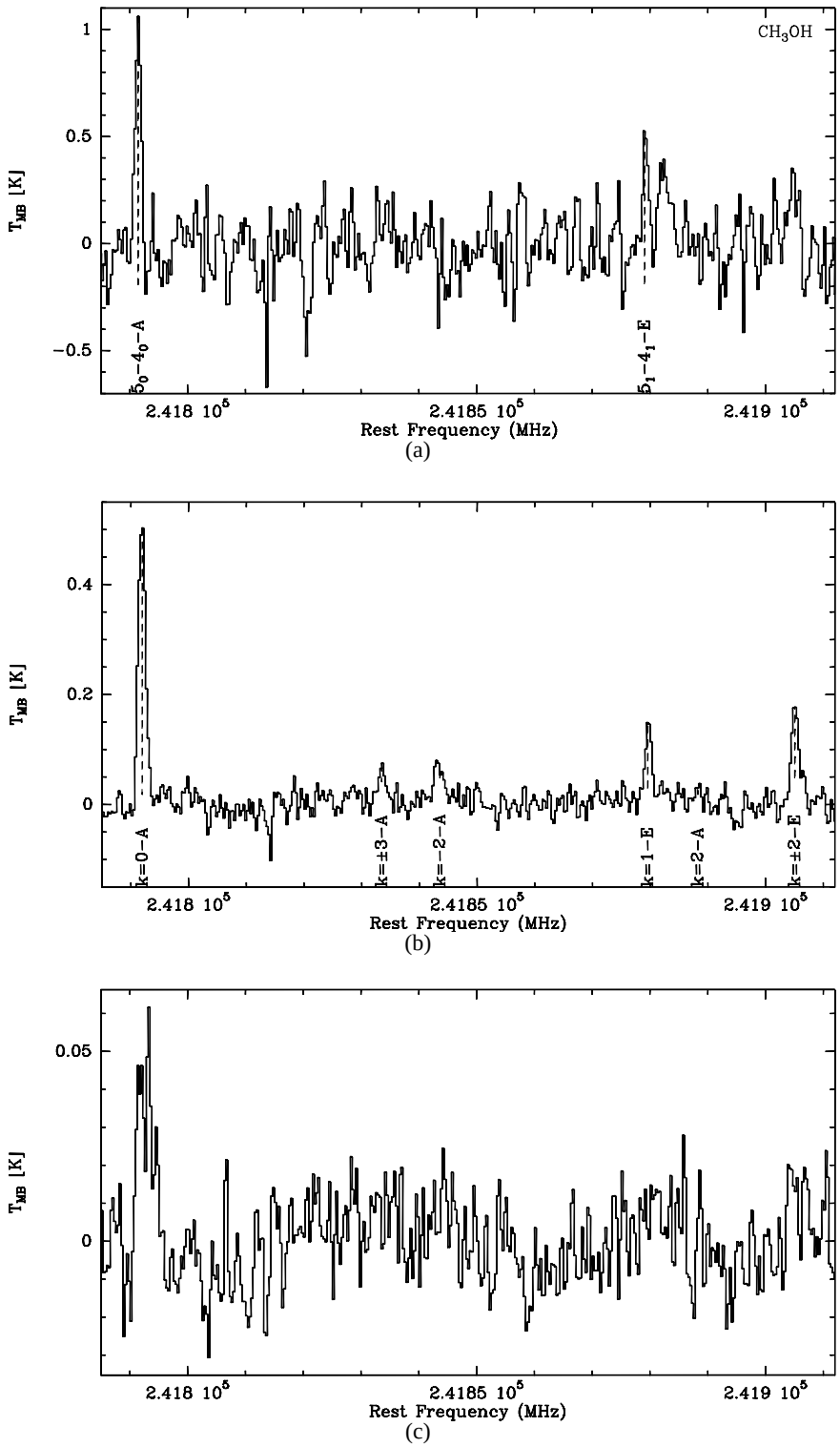

Fig. 4. Spectrum of the CH_3OH ($5_k - 4_k$) band towards clump 1 at a resolution of $\sim 10''$ (top), smoothed to a resolution of $\sim 20''$ (middle), and averaged over the interclump medium (bottom). Data are from the IRAM-30m telescope.

to 0.77 km s^{-1}) show that clump 1 peaks around 9.5 km s^{-1} and clump 3 around 10.5, as for $H^{13}CN$ (Lis & Schilke 2003). The secondary peak detected to the northeast of clump 1 has a peak velocity around 11 km s^{-1}, while the molecular cloud to the south of the Bar is red-shifted with respect to the clumps ($v_{lsr} \sim 8$ km s^{-1}). This trend in velocity (blue-shifted velocities in the northeast, red-shifted values in the southwest) was also found by Young Owl et al. (2000) in their HCN maps.

3.2. Hybrid interferometric+single-dish data

Figure 8 compares the 30m (top panels) and hybrid 30m+PdBI (bottom panels) data cubes. The left column displays the images

Table 2. Line parameters

	T_{MB} [K]	$\int T_{MB} dv$ [km s^{-1}]	Δv^a [km s^{-1}]	T_{MB} [K]	$\int T_{MB} dv$ [K km s^{-1}]	Δv^a [km s^{-1}]
	H_2CO ($3_{0,3} - 2_{0,2}$)			CH_3OH ($5_0 - 4_0$-A)		
clump 1	3.2	8.9	2.0	1.1	1.8	1.4
interclump	0.3	1.2	3.1	0.06	0.2	4.0

[a] corrected for the spectral resolution, $\Delta v = \sqrt{(\Delta v_{obs})^2 - (\Delta v_{res})^2}$

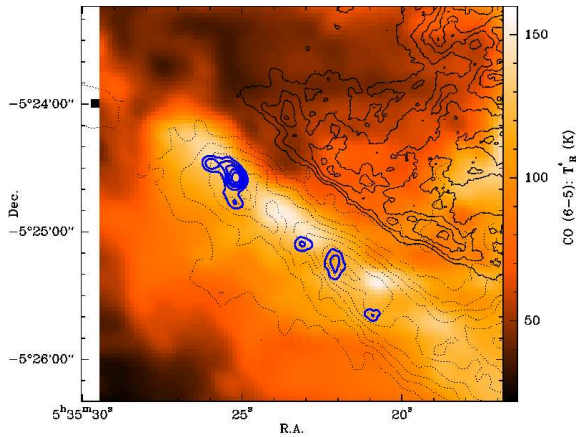

(a)

Fig. 5. Distribution of the CO(6-5) peak brightness temperature (colour image). The black contours (from 40% of the peak intensity, in steps of 10%) show the 20 cm continuum emission, which traces the ionisation front. The dotted contours (from 15% of the peak intensity, in steps of 10%) are the integrated intensity of the H_2CO $3_{0,3} - 2_{0,2}$ line; the blue contours (as in Fig. 1) represent the dense clumps; the square marks the position of the secondary peak identified in H_2CO and CH_3OH.

integrated between 8.3 and 11.7 km/s. The middle column displays the spectra averaged over the whole interferometric field-of-view. The hybrid spectra are identical to the 30m ones within the noise level, confirming that all the extended emission filtered out by the PdBI is correctly recovered from the single-dish data. The right column of Fig. 8 displays the spectra averaged over the central clump marked in the left column. The hybrid spectrum is brighter than the 30m spectrum implying beam dilution in the single-dish data.

From the PdBI data and the hybrid 30m+PdBI data, we can therefore conclude that the H_2CO emission comes from both an extended component and a compact one, still unresolved at the resolution of the IRAM-30m telescope.

4. Discussion

4.1. Formaldehyde

Line ratios of formaldehyde lines can be used to infer the physics of the gas in dense molecular regions (Mangum & Wootten 1993). Because of the coarse spectral resolution of our observations ($\Delta v \sim 1.7$ km s^{-1}), the line profiles of the H_2CO transitions are poorly resolved. As a result, we do not have a correct measure of the peak intensity of the lines, diluted over the beam, but our values are a lower limit to the true main-beam line intensities. However, the areas are conserved quantities and can be used to study the excitation of H_2CO in the Orion Bar.

Figure 9 shows the ratio of the integrated intensities of the $3_{0,3} - 2_{0,2}$ line to the $3_{2,2} - 2_{2,1}$ line. The analysis is limited to the region where the signal-to-noise ratio of the $3_{2,2} - 2_{2,1}$ integrated intensity is at least equal to 3. The ratio increases from the northeast, where the clumps are, to the southwest.

We ran LVG calculations for column densities of H_2CO between 10^{12} and 10^{15} cm^{-2}, temperatures in the range 20–200 K, and densities of 10^4–10^8 cm^{-3}, and calculated the behaviour of the χ^2 value of the observed $3_{0,3} - 2_{0,2}$ and $3_{2,2} - 2_{2,1}$ line intensities as function of these quantities. Two possible regimes are found (see Fig. 10), independent of temperature. At low densities (n$< 10^6$ cm^{-3}), the χ^2 value depends only on the product of the H_2 density and H_2CO column density (low-density branch). For higher densities, the χ^2 value varies only slowly with H_2 density and is mostly a function of H_2CO column density (high-density branch).

For the values in the interclump gas, assuming a beam filling factor of unity, we find a nominal minimum for the interclump medium at $T = 180$ K, n(H_2) $= 6.6 \times 10^5$ cm^{-3}, $N_{H_2CO} = 1.4 \times 10^{13}$ cm^{-2}. However, as can be seen in Fig. 10, these parameters are not well constrained. Using the 1σ confidence level, we derived a lower limit to the kinetic temperature of the interclump equal to 76 K, and the product $n_{H_2} \times N_{H_2CO}$ is equal to $\sim 3 \times 10^{18}$ cm^{-5} for densities smaller than 10^6 cm^{-3}. By comparison with PDR models, Young Owl et al. (2000) found densities of hydrogen nuclei of 10^4-10^5 cm^{-3} in the interclump; similarly, Hogerheijde et al. (1995) found an interclump H_2 density of 3×10^4 cm^{-3} by modelling mm line observations. Thus, by using a molecular hydrogen density between 5×10^3 and 5×10^4 cm^{-3} we can constrain the column density of H_2CO to values in the range $6 \times 10^{13} - 6 \times 10^{14}$ cm^{-2}. The high-density branch does not appear to be relevant for the interclump medium.

In Sect. 3.2 we analysed the combined PdBI+30m data and concluded that the H_2CO emission is composed of two components, one extended and one unresolved at the resolution of the 30m telescope at this frequency. However from these data, it is difficult to infer the exact size of clump 1 and the contribution of the interclump gas to the total emission of H_2CO. In Fig. 8, we marked clump 1 with an ellipse of $15'' \times 5''$ (P.A.=47°) and showed that the IRAM-30m data are affected by beam dilution at this scale, implying a smaller size for the clump. Therefore, for clump 1, we corrected the main-beam line intensities for the contribution from the interclump and for the beam dilution assuming a typical size for the clump of $7''$ (see Lis & Schilke 2003). As expected given the similar value of the line ratio on clump 1 and in the interclump, the values derived are similar to those of the interclump: $T = 170$ K, n(H_2) $= 6.6 \times 10^5$ cm^{-3}, $N_{H_2CO} = 1.6 \times 10^{14}$ cm^{-2}. The 1σ contour gives a value of 3.8×10^{19} cm^{-5} for the product $n_{H_2} \times N_{H_2CO}$ for $N_{H_2CO} > 5 \times 10^{13}$ cm^{-2} and $n(H_2) < 5 \times 10^5$ cm^{-3}. For the low-density branch, we derive a lower limit of 50 K for the kinetic temperature. For the high-density branch, more appropriate for the clump, the column den-

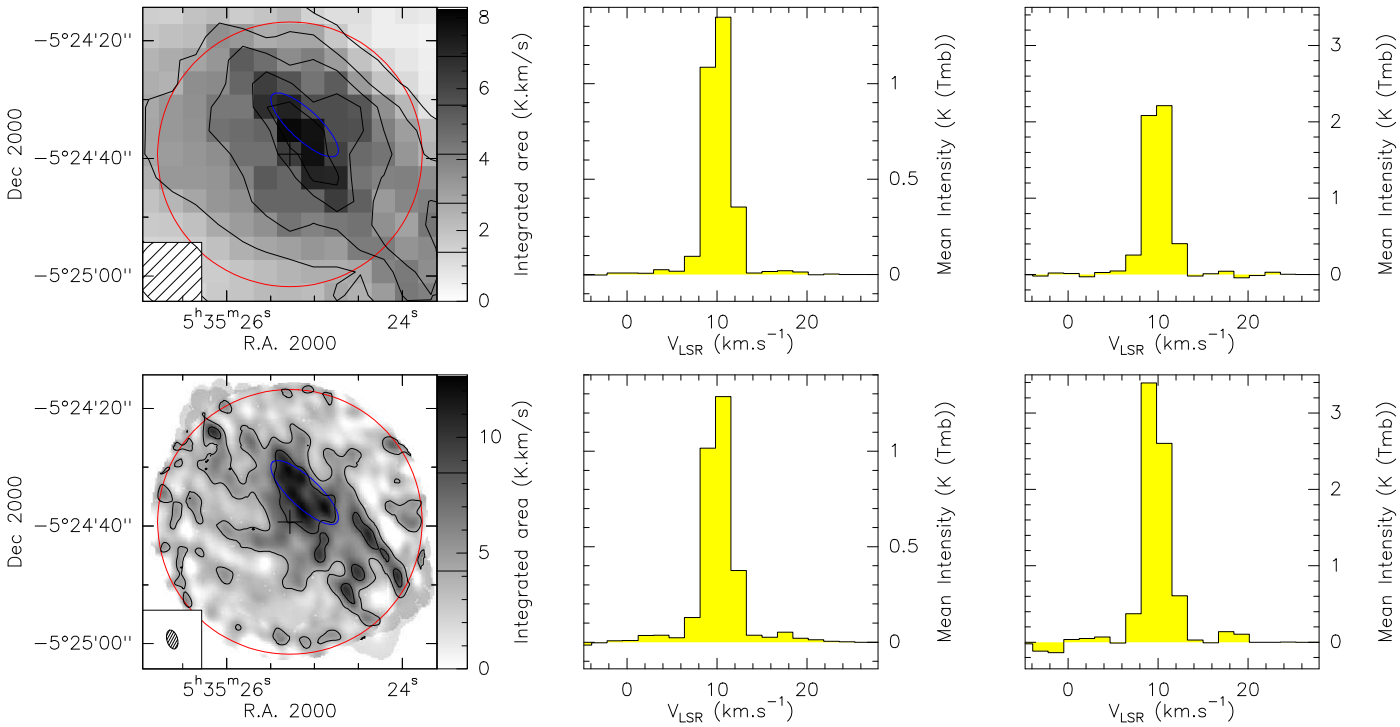

Fig. 8. *Top line:* IRAM-30m data. *Bottom line:* hybrid 30m+PdBI deconvolved data cube. *Left column:* Images of the integrated line intensity of the H_2CO ($3_{0,3} - 2_{0,2}$) transition between 8.3 and 11.7 km/s. The values of the contour levels are shown on the colour scale. *Middle column:* Spectra averaged over the whole interferometric field-of-view marked as the red circle on the images. *Right column:* Spectra averaged over the central clump marked with the blue ellipse on the images.

sity is constrained to values $2.8\times10^{14} - 5.4\times10^{14}$ cm^{-2}. A lower limit of 80 K can be derived for the kinetic temperature. It may appear surprising that the temperature is so little constrained, although the ratio of these lines has been used as a temperature tracer (Mangum & Wootten 1993; Hogerheijde et al. 1995). However, for the values of the line ratio we observe, the LVG predictions show a more complex behaviour with temperature (see also Fig. 13 of Mangum & Wootten 1993). Taking the measurement errors into account by calculating the χ^2 value, as we do, and using the line intensities and not just the line ratios then constrains only a lower limit to the temperature.

The results of the LVG analysis of H_2CO are presented in Table 3.

4.2. Methanol

Leurini et al. (2004) have studied the excitation of the CH_3OH ($5_k - 4_k$) band as function of the temperature, density, and methanol column density of the gas for a range of physical conditions applicable to the Orion Bar. They concluded that line ratios within this band are not sensitive to the temperature of the gas for temperatures higher than 30 K, but only depend on the density.

The methanol emission from clumps 1 and 3 is studied in a separate paper (Parise et al. 2009): clump 1 is found to be warmer than clump 3, although the errors are large (3σ ranges: $T_1 \sim 45^{+47}_{-17}$ K, $T_3 \sim 35^{+17}_{-15}$ K), but with similar column densities and densities ($N_{CH_3OH} \sim 3\times10^{14}$ cm^{-2}, $n \geq 5\times10^6$ cm^{-3}). These values were derived by modelling the $5_k - 4_k$ and $6_k - 5_k$ bands observed with the IRAM-30m (observations presented in this paper) and the APEX telescopes, respectively. For the models, the IRAM data were smoothed to the resolution of the APEX data (*FWHM* beam ∼ 20″). A source size of 10″ was used, since several clumps fall in the beam of the observations. This is equivalent to assuming that all clumps have similar physical conditions. Since the CH_3OH emission was found to be optically thin, we can correct the results for a source size of 7″ (as assumed for the model of H_2CO) and derive the equivalent column density. This corresponds to a total column density of 5.4×10^{14} cm^{-2}, or to 2.7×10^{14} cm^{-2} for CH_3OH-*A*, assuming that the two symmetric states have the same column density. The 1σ confidence level is $2.3 \times 10^{14} - 3.1 \times 10^{14}$ cm^{-2}.

For the interclump medium, we analysed the CH_3OH spectrum averaged over the area of the interclump medium outlined in Fig. 5. We ran models for the excitation of methanol in the range of densities $10^4 - 10^8$ cm^{-3}, column densities $10^{12} - 10^{18}$ cm^{-2}, and temperatures 20 – 200 K. The observed main-beam brightness temperature of the ($5_0 - 4_0$)-*A* line in the interclump medium is 0.06 ± 0.01 K. Assuming that the emission comes from an extended source (e.g., beam filling factor $\eta_c = 1$), we find a situation similar to the one described for H_2CO and we can identify two different regimes. In the first ($n < 10^6$ cm^{-2}), a fit to the data is found for $N_{CH_3OH-A} < 1.3 \times 10^{14}$ cm^{-2}: the column density decreases with increasing density, but their product is almost constant (between 2×10^{17} cm^{-5}, 50 K ≤ T < 200 K, and 2×10^{18} cm^{-5}, 20 K < T < 50 K). For higher densities, the $5_0 - 4_0$ line thermalises. In this regime, the column density increases slowly ($N_{CH_3OH-A} = 1.3 \times 10^{12} - 2 \times 10^{13}$ cm^{-2}). For both regimes, the dependence on the kinetic temperature is not strong and the results presented are valid for temperatures in the range 20–200 K. However, increasing the temperature of the gas implies a decrease in the column density of methanol for the low-density case ($T \geq 50$ K, $N_{CH_3OH-A} < 3 \times 10^{13}$ cm^{-2}, see Fig. 11).

As already discussed in the previous section, from the literature we know that the density of the interclump gas is less than

Table 3. Summary of the model results

	N_{H_2CO-p} [10^{13} cm^{-2}]	N_{CH_3OH-A} [10^{13} cm^{-2}]	$[CH_3OH-A]/[H_2CO-p]$
clump 1	$(28-54)^a$	$23-31$	$0.4-1.1$
interclump	$(6-60)^b$	$(0.04-4)^b$	$7\times10^{-4}-0.7$
		$(0.04-0.4)^c$	$(7\times10^{-4}-7\times10^{-2})^c$

[a] assuming $n = 10^6$ cm^{-3}
[b] assuming $n = (5\times10^3 - 5\times10^4)$ cm^{-3}
[c] assuming $T > 50$ K

10^6 cm^{-3}, and therefore that the low-density regime applies to the modelling of the interclump. The best fit to the data is found for $N_{CH_3OH-A} \sim 3\times10^{12}$ cm^{-2}, $T \sim 80$ K, $n \sim 9\times10^4$ cm^{-3}. For densities in the range $5\times10^3 - 5\times10^4$ cm^{-3}, and for the values of the product $N\times n$ given above, we derive column densities in the range $4\times10^{11} - 4\times10^{13}$ cm^{-2}. However, if we allow only temperatures above 50 K, as found in our data and by other authors, the inferred methanol column density in the interclump is $4\times10^{11} \leq N \leq 4\times10^{12}$ cm^{-2} (see Table 3).

5. Abundances of methanol and formaldehyde in the Orion Bar

From the analysis performed in the previous section, we can compute the abundance of methanol relative to formaldehyde in the interclump medium and in the dense clumps, and verify that the drop of intensity of the methanol emission in the interclump medium is the result of the different physics of the interclump relative to the dense clumps, or whether it reflects a real decrease in the CH_3OH abundance.

Given an estimate of H_2 column density, we could also infer the abundance of both molecules relative to molecular hydrogen. An estimate of the H_2 column density can be derived from the continuum emission at (sub)millimetre wavelengths, assuming a given temperature for the dust and optically thin emission. The continuum emission at 350 μm of the Orion Bar was studied by Lis et al. (1998). These authors defined an average temperature for the dust in the OMC-1 region of 55 K on the basis of its FIR colours (Werner et al. 1976) and excluded colder temperatures for the Orion Bar given the good agreement of the 350 μm continuum emission and the CO(6-5) emission, which originated in the outer PDR layers. However, Werner et al. (1976) found an average FIR colour temperature of 75 K in the Orion Bar, which could imply that the Orion Bar is significantly warmer than the rest of OMC-1. For a dust temperature of 55 K in the interclump medium, and for the mean value of the 350 μm emission over the region used to derive the average spectra of the interclump medium (Fig. 1), we derive a column density of H_2 of 5.3×10^{21} cm^{-2}. This translates into to 3.4×10^{21} cm^{-2} for $T_d = 75$ K. A value of 0.101 g cm^{-2} was used for the dust opacity (Ossenkopf & Henning 1994). For clump 1, for a temperature of 45 K (as derived from methanol), and under the assumption that the dust and the gas are thermally coupled at the high density of the clumps (e.g., Krügel & Walmsley 1984), the H_2 column density is 2×10^{23} cm^{-2}. This is not the average column density on the beam, but it was corrected for a source size of 7″ and for the contribution of the interclump medium at the position of clump 1. These values translate into abundances of H_2CO in the range $(11-110)\times10^{-9}$ for the interclump,$(1.4-2.7)\times10^{-9}$ for the clumps. For methanol, we obtain an abundance relative to H_2 of $(0.08-8)\times10^{-9}$ for the interclump, $(1.2-1.6)\times10^{-9}$ for the clumps.

However, these estimates are affected by large uncertainties: a difference of 20 K in the dust temperature implies an uncertainty of a factor of ~ 2 in the estimate of the H_2 column density in the interclump, uncertainty that could be even greater if the average temperature in the region of the interclump used in our analysis is higher than 75 K. Similarly, the estimate of the H_2 column density on the clumps is affected by large uncertainties because of the assumption that the dust is thermally coupled to the gas at high densities and because of the large errors on the temperature of the gas from the methanol spectrum ($28 < T_1 < 92$ K, $20 < T_3 < 52$ K).

On the other hand, the uncertainties in the determination of the abundance of CH_3OH relative to H_2CO are related only to the errors in the estimate of the column density of the two molecules, which already include the uncertainties in the temperature. Therefore, we believe $[CH_3OH-A]/[H_2CO-p]$ to be more solidly estimated than $[CH_3OH-A]/[H_2]$ or $[H_2CO-p]/[H_2]$. Using the column densities derived in the previous section, we infer an abundance of CH_3OH relative to H_2CO of the order 0.4–1.1 in the dense clumps, and 7×10^{-4}– 7×10^{-1} in the interclump. If we assume that the temperature of the interclump medium is higher than 50 K, then abundance of methanol drops down to 7×10^{-4}– 7×10^{-2}. Since it is a reasonable assumption that the temperature of the interclump medium is 50 K or even higher, we conclude that the abundance of methanol relative to formaldehyde decreases by at least one order of magnitude in the interclump medium in comparison to the dense clumps.

A possible explanation for the decrease in abundance of methanol relative to formaldehyde from the clumps to the interclump medium is photodissociation in a low-density enviroment. Although the photodissociation rates of CH_3OH and H_2CO are of the same order of magnitude (Le Teuff et al. 2000), one of the products of the photodissociation of methanol is formaldehyde. Therefore, both molecules can be destroyed by the radiation field in the interclump medium, but H_2CO may be replenished through the photodissociation of CH_3OH. However, large uncertainties affect the measurement of the photodissociation rates, and so more accurate models would be required to test this hypothesis. Alternatively, as already discussed by Leurini et al. (2006), H_2CO could be formed in the interclump medium through gas phase reactions, which are not efficient for the formation of CH_3OH (Luca et al. 2002).

6. Conclusion

In a previous analysis of methanol and formaldehyde towards the Orion Bar, we suggested that the two molecules might trace different environments and that, while CH_3OH is associated with the clumpy molecular cores of the Bar, H_2CO is found in the in-

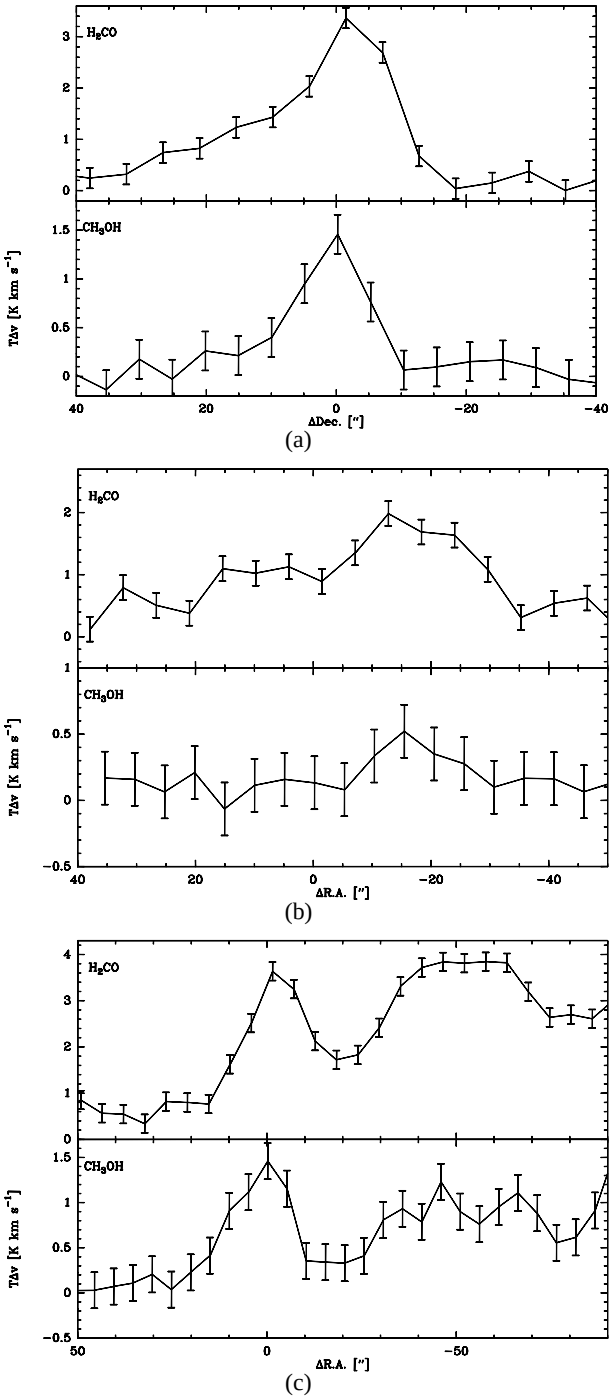

Fig. 6. Variation in the integrated intensity of the CH_3OH-*A* ($5_0 - 4_0$) and H_2CO $3_{2,2} - 2_{2,1}$ lines observed with the IRAM-30m telescope across clumps 1 (**a**), the interclump medium between clump 1 and 2 (**b**) and along the Bar (**c**). In Fig. 1 we outline the strips used to extract the plots.

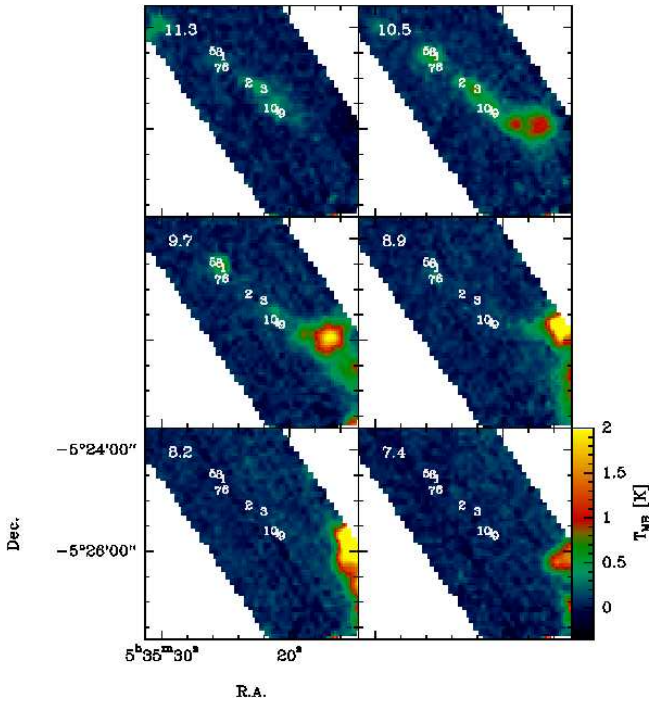

Fig. 7. Channel maps of the CH_3OH-*A* ($5_0 - 4_0$) emission between 11.3 and 7.4 km s^{-1} observed with the IRAM-30m telescope.

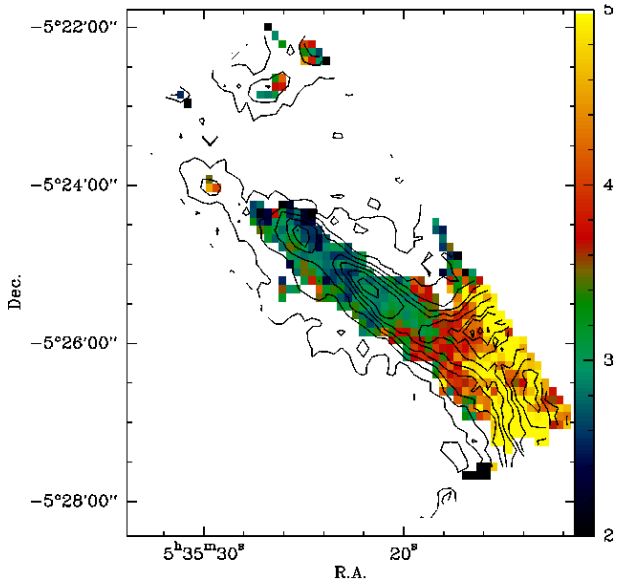

Fig. 9. Ratio of the integrated intensity of the H_2CO $3_{0,3} - 2_{0,2}$ transition to the $3_{2,2} - 2_{2,1}$. The solid black contours show the integrated intensity of the $3_{0,3} - 2_{0,2}$ line (levels are from 1.8 K km s^{-1} in steps of 1.8). Typical errors along the Bar are of the order of 0.3.

terclump material. To test this hypothesis, we mapped the Orion Bar in both molecular species with the IRAM-30m telescope, with a spatial resolution slightly higher than the expected size of the clumps. Additional data were taken with the IRAM Plateau de Bure Interferometer in H_2CO.

Both molecules are detected in the Orion Bar in our single-dish data. Our data show that CH_3OH peaks towards the clumps of the Bar, but its intensity decreases below the detection threshold in the interclump at individual positions. By averaging over a large region of the interclump medium, the strongest of the CH_3OH lines in our setup ($5_0 - 4_0$-*A*) is detected with a peak intensity of ~ 0.06 K. On the other hand, contrary to the hypothesis formulated in our previous study, formaldehyde is detected towards the clumps and the interclump gas.

Using an LVG program, we studied the excitation of H_2CO and CH_3OH in the Orion Bar. We suggest that formaldehyde is

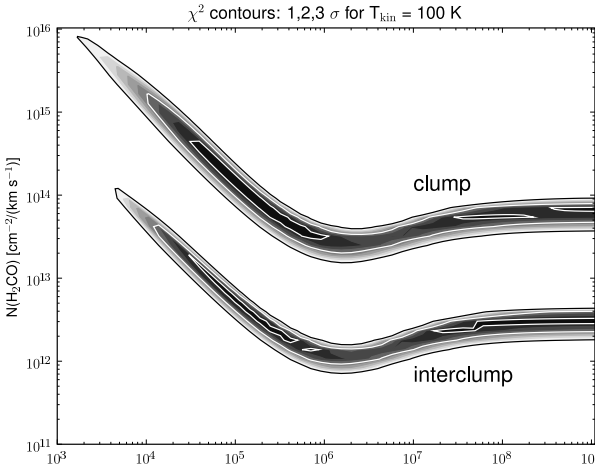

Fig. 10. χ^2 square distribution of the $3_{0,3} - 2_{0,2}$ and $3_{2,2} - 2_{2,1}$ line intensities in the [$n(H_2)$, $N(H_2CO)$] plane for a temperature of 100 K for the two sets of observations clump and interclump shown in Fig. 3. The plot shows, for each spatial region, the low-density branch and the high-density branch discussed in the text. Note that to derive the column densities given in § 4.1, one has to multiply with the line widths.

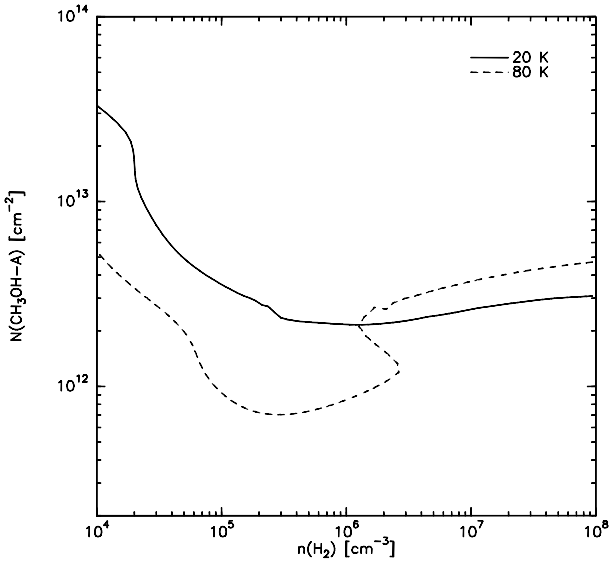

Fig. 11. Results of the statistical equilibrium calculations for CH_3OH. The solid and dashed lines show the line intensity of the $5_0 - 4_0$-*A* line as measured towards the interclump medium (0.06 K) for temperatures of 20 and 80 K, respectively, as functions of density and column density of CH_3OH-*A* .

present in both components of the Bar (clumps and interclump material), with column densities up to 5.4×10^{14} cm^{-2} in the clumps and between $6 \times 10^{13} - 6 \times 10^{14}$ cm^{-2} in the interclump. These values only refer to para-formaldehyde. From the analysis of methanol, we concluded that the reason for the drop of intensity of CH_3OH in the interclump medium is not the different physical conditions with respect to the clumps, but a real drop in its column density compared to the clumps (down to 4×10^{11} cm^{-2} for temperatures above 50 K). The abundance of methanol relative to formaldehyde decreases by at least one order of magnitude in the interclump medium compared to that in the dense clumps.

Despite the large errors on our estimates, our observations reveal that the column density of methanol and formaldehyde in the clumps are of the same order of magnitude, while the column density of methanol in the interclump is lower than that of formaldehyde. This may be a result of photodissociation of CH_3OH in the unshielded interclump gas, or it may reflect that H_2CO can be produced in the gas phase more efficiently than CH_3OH. Definitive observational conclusions would require a much deeper integration towards the interclump gas and a better characterisation of its density and temperature. More detailed chemical models of PDRs, including grain surface reactions, are clearly needed to properly interpret these observational results.

Acknowledgements. We are grateful to Helmut Wiesemeyer for his support before and during the observations, and to the observers who obtained part of the data presented in this work during pooled observations at the IRAM-30m telescope.

References

Gorti, U. & Hollenbach, D. 2002, ApJ, 573, 215
Gueth, F., Guilloteau, S., & Viallefond, F. 1995, in The XXVIIth Young European Radio Astronomers Conference, ed. D. A. Green & W. Steffen, 8
Hidaka, H., Watanabe, N., Shiraki, T., Nagaoka, A., & Kouchi, A. 2004, ApJ, 614, 1124
Hogerheijde, M. R., Jansen, D. J., & van Dishoeck, E. F. 1995, A&A, 294, 792
Jansen, D. J., Spaans, M., Hogerheijde, M. R., & van Dishoeck, E. F. 1995, A&A, 303, 541
Krügel, E. & Walmsley, C. M. 1984, A&A, 130, 5
Le Teuff, Y. H., Millar, T. J., & Markwick, A. J. 2000, A&AS, 146, 157
Leurini, S., Rolffs, R., Thorwirth, S., et al. 2006, A&A, 454, L47
Leurini, S., Schilke, P., Menten, K. M., et al. 2004, A&A, 422, 573
Lis, D. C. & Schilke, P. 2003, ApJ, 597, L145
Lis, D. C., Serabyn, E., Keene, J., et al. 1998, ApJ, 509, 299
Luca, A., Voulot, D., & Gerlich, D. 2002, in WDS'02 Proceedings of Contributed Papers, Part II, Safrankova (ed), Matfyzpress, 294
Mangum, J. G. & Wootten, A. 1993, ApJS, 89, 123
Ossenkopf, V. & Henning, T. 1994, A&A, 291, 943
Parise, B., Leurini, S., Schilke, P., Roueff, E., Thorwirth, S., & Lis, D. C. 2009, A&A, 508, 737
Pety, J. 2005, in SF2A-2005: Semaine de l'Astrophysique Francaise, ed. F. Casoli, T. Contini, J. M. Hameury, & L. Pagani, 721–722
Rodríguez-Fernández, N. J., Pety, J., & Gueth, F. 2008, Single-dish observation and processing to produce the short-spacing information for a millimeter interferometer, IRAM memo 2008-2
Schilke, P., Pineau des Forêts, G., Walmsley, C. M., & Martín-Pintado, J. 2001, A&A, 372, 291
Schuster, K.-F., Boucher, C., Brunswig, W., et al. 2004, A&A, 423, 1171
Tauber, J. A., Lis, D. C., Keene, J., Schilke, P., & Buettgenbach, T. H. 1995, A&A, 297, 567
Tielens, A. G. G. M., Meixner, M. M., van der Werf, P. P., et al. 1993, Science, 262, 86
van der Werf, P. P., Stutzki, J., Sternberg, A., & Krabbe, A. 1996, A&A, 313, 633
van der Wiel, M. H. D., van der Tak, F. F. S., Ossenkopf, V., et al. 2009, ArXiv e-prints
Werner, M. W., Gatley, I., Becklin, E. E., et al. 1976, ApJ, 204, 420
Young Owl, R. C., Meixner, M. M., Wolfire, M., Tielens, A. G. G. M., & Tauber, J. 2000, ApJ, 540, 886
Yusef-Zadeh, F. 1990, ApJ, 361, L19